Nanoparticle Assembly of Ordered Multicomponent Mesostructured Metal Oxides via a Versatile Sol−Gel Process

Jie Fan, Shannon W. Boettcher, and Galen D. Stucky*

Department of Chemistry and Biochemistry, University of California, Santa Barbara, California 93106

Received October 3, 2006. Revised Manuscript Received October 27, 2006

Multicomponent metal oxides have attracted attention for their potential use in electronic, (photo)-catalytic, photovoltaic, and energy storage applications. The ability to simultaneously control the nanoscale structure and composition of such materials using simple and inexpensive routes is important for that potential to be realized. Here we introduce a simple and widely applicable methodology for the synthesis of multicomponent mesostructured metal oxides (MMMOs) from the combination of inexpensive and commercially available polymers with metal alkoxides solubilized in a sol−gel solution consisting of acetic acid, hydrochloric acid, and ethanol (AcHE). MMMOs obtained utilizing the AcHE system have tunable pore structures, a high degree homogeneity, and in certain cases thermal stability above 1000 °C. The ability to easily process these diverse MMMOs in the form of thin films, free-standing membranes, and monoliths provides distinct advantages over previously reported MMO synthesis procedures—especially when large quantities of material are required, for instance, in heterogeneous catalyst development. Most importantly, we demonstrate that the controlled binding of reactive metal ions with acetic acid in the AcHE solution yields nanometer-sized particles for a diverse collection of inorganic materials with homogeneous condensation kinetics. This allows for the simple synthesis of complicated and novel MMMO compositions (e.g., rare earth and mixed transition metal oxides) via cooperative assembly with amphiphilic block copolymers. The development of such simple and widely applicable methodologies are extremely important for the practical implementation of porous metal oxides.

Introduction

Metal oxides (MOs) have emerged as a promising class of new materials whose compositional and structural diversity leads to an array of unique chemical and physical properties.[1] Indeed, many MOs with advanced properties such as selective oxidation, electron or ionic percolation, and energy transfer are multicomponent systems having two or more types of metal cations.[2,3] Furthermore, the ability to fabricate porous mesostructured films, powders, and monoliths from these materials is extremely important for applications in which high interfacial surface area is important, for example, in heterogeneous catalysts, energy storage, photocatalysis, or nanostructured photovoltaics.[4−6] One promising route to rationally control the mesoscale structure of such oxides is through the use of structure-directing amphiphilic block copolymers.[7−11] This cooperative assembly route was originally developed for the synthesis of mesostructured silica where the simple and effective control over silicate condensation kinetics has allowed for the creation of an enormous variety of mesostructures.[12−14] The ability to tune the condensation kinetics of a wide variety of MO components, in a way analogous to the "benchmark" silica case where the kinetics of inorganic growth and inorganic−organic co-assembly processes are matched (Figure 1), is an important goal. Although several routes for the synthesis of mesostructured metal oxides (MMOs) have been developed,[7−9,15,16] a simple and broadly applicable synthetic methodology remains a challenge due to the dissimilar condensation kinetics and chemistry of the MO precursors, which often leads to undesirable macro-scale phase separation that disrupts the co-assembly process.[17,18]

* To whom correspondence should be addressed. E-mail: stucky@chem.ucsb.edu.

(1) Fierro, J. L. G. *Metal Oxides: Chemistry and Applications*; CRC Press: Boca Raton, 2006.
(2) Carreon, M. A.; Guliants, V. V. *Eur. J. Inorg. Chem.* **2005**, 27−43.
(3) Morris, C. A.; Anderson, M. L.; Stroud, R. M.; Merzbacher, C. I.; Rolison, D. R. *Science* **1999**, *284*, 622−624.
(4) Corma, A. *Chem. Rev.* **1997**, *97*, 2373−2419.
(5) Nozik, A. J. *Physica E* **2002**, *14*, 115−120.
(6) Bartl, M. H.; Boettcher, S. W.; Frindell, K. L.; Stucky, G. D. *Acc. Chem. Res.* **2005**, *38*, 263−271.
(7) Yang, P. D.; Zhao, D. Y.; Margolese, D. I.; Chmelka, B. F.; Stucky, G. D. *Nature* **1998**, *396*, 152−155.
(8) Tian, B. Z.; Liu, X. Y.; Tu, B.; Yu, C. Z.; Fan, J.; Wang, L. M.; Xie, S. H.; Stucky, G. D.; Zhao, D. Y. *Nat. Mater.* **2003**, *2*, 159−163.
(9) Grosso, D.; Boissiere, C.; Smarsly, B.; Brezesinski, T.; Pinna, N.; Albouy, P. A.; Amenitsch, H.; Antonietti, M.; Sanchez, C. *Nat. Mater.* **2004**, *3*, 787−792.
(10) Goltner, C. G.; Antonietti, M. *Adv. Mater.* **1997**, *9*, 431 ff.
(11) Brezesinski, T.; Antonietti, M.; Groenewolt, M.; Pinna, N.; Smarsly, B. *New J. Chem.* **2005**, *29*, 237−242.
(12) Kresge, C. T.; Leonowicz, M. E.; Roth, W. J.; Vartuli, J. C.; Beck, J. S. *Nature* **1992**, *359*, 710−712.
(13) Zhao, D. Y.; Feng, J. L.; Huo, Q. S.; Melosh, N.; Fredrickson, G. H.; Chmelka, B. F.; Stucky, G. D. *Science* **1998**, *279*, 548−552.
(14) Che, S.; Garcia-Bennett, A. E.; Yokoi, T.; Sakamoto, K.; Kunieda, H.; Terasaki, O.; Tatsumi, T. *Nat. Mater.* **2003**, *2*, 801−805.
(15) Schuth, F. *Chem. Mater.* **2001**, *13*, 3184−3195.
(16) Boettcher, S. W.; Bartl, M. H.; Hu, J. G.; Stucky, G. D. *J. Am. Chem. Soc.* **2005**, *127*, 9721−9730.
(17) Brinker, C. J.; Sherer, G. W. *Sol-Gel Science*; Academic Press: San Diego, CA, 1990.
(18) Livage, J.; Henry, M.; Sanchez, C. *Prog. Solid State Chem.* **1988**, *18*, 259−341.

10.1021/cm062359d CCC: $33.50
Published on Web 12/19/2006

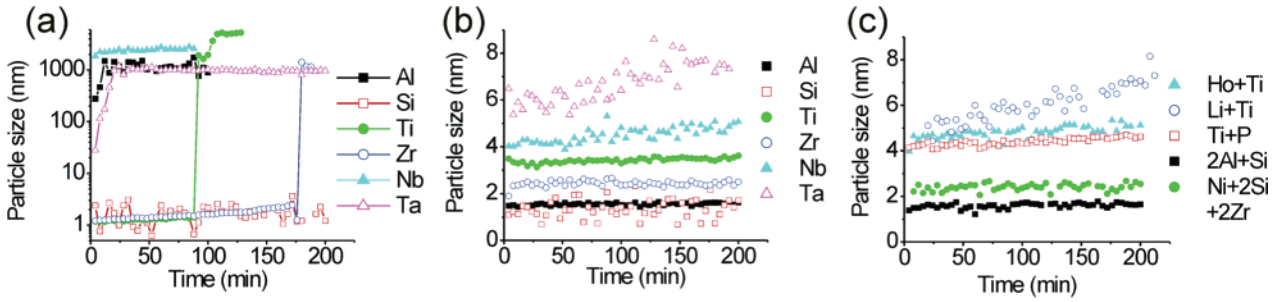

Figure 1. Evolution of particle sizes of isolated metal alkoxides at ambient conditions (25 °C, RH ~ 50%) in (a) EtOH (100%) and (b) HOAc−HCl−EtOH solution. The concentration of the metal source is fixed at 0.5 M. The relative concentrations of HOAc and HCl are varied with respect to the type of metal source. M/HOAc/HCl is 1:4:*x*, where $x = 1.2$ when M is Al, Si, Ti, Nb; $x = 2.4$ when M is Zr; $x = 1.8$ when M is Ta (Al, aluminum ethoxides; Si, tetraethyl silicates; Ti, titanium butoxides; Zr, zirconium butoxides; Nb, niobium ethoxides; Ta, tantalum ethoxides). (c) The size evolution of mixed metal species (Li, lithium chloride; Ni, nickel (II) nitrate; Ho, holmium chloride; P, triethyl phosphate).

Here we introduce an alternative broadly applicable sol−gel system for the preparation of homogeneous, ordered, thermally stable, multicomponent mesoporous metal oxides (MMMOs). The growth kinetics of various metal alkoxides are controlled by the judicious addition of complexing ligands such that the particle size and condensation kinetics of quite different precursors are matched: this allows for complex MO stoichiometries. The sol−gel solution consists of three components. (1) Acetic acid acts as a complexing agent to modify the condensation kinetics of metal alkoxides.[19,20] (2) The controlled addition of a strong aqueous acid such as HCl or HNO_3 partially hydrolyzes and charges the modified inorganic precursor to enhance the affinity for the hydrophilic block of the block copolymer. Furthermore, these strong acids may act as charge intermediates between surfactants and inorganic species and inhibit condensation of certain metal ions. (3) An amphoteric solvent such as ethanol or acetic acid ensures sufficient solubility of all species involved in the assembly process. For simplification, this system is denoted as AcHE, where Ac, H, and E represent acetic acid, HCl, and EtOH, respectively. When a selection of metal species stabilized in the AcHE solution is combined with a suitable structure-directing block-copolymer template, MMMOs with a range of compositions and structures can be easily and reproducibly obtained.

Experimental Section

Methods. The synthesis is similar to the procedure for the preparation of mesoporous silica,[21] except for the introduction of acetic acid and MO precursors. In a typical synthesis of a mesostructured membrane (e.g., ZrO_2), 10 mmol of $Zr(OBu)_4$, 40 mmol of HOAc, 24 mmol of HCl (or HNO_3), and 1.6 g of F127 ($EO_{96}PO_{70}EO_{96}$, MW = 12 000 g/mol) were dissolved in 30 mL of ethanol. The mixture was stirred vigorously for 1 h and transferred into a Petri dish (diameter 125 mm). The ethanol was evaporated at 40 °C with a relative humidity ~40% (relative humidity ranging from 10% to 80% did not substantially affect the mesostructure, in contrast to other reported methods).[22] After 12 h, a transparent membrane was formed, and it was transferred into a 65 °C oven and aged for an additional 24 h. As-synthesized mesostructured hybrids were calcined at 350 °C in air for 5 h (ramp rate 2 °C/min) to obtain mesoporous membranes.

For the synthesis of multicomponent MOs, ethanol-soluble metal salts (nitrates, acetates, or chlorides) together with metal alkoxides are used as the precursors. For example, in the synthesis of mesoporous $NiO-2SiO_2-2ZrO_2$, 5 mmol of $Ni(NO_3)_2 \cdot 6H_2O$, 10 mmol of tetraethylorthosilicate, 10 mmol of $Zr(OBu)_4$, 40 mmol of HOAc, 24 mmol of HCl (or HNO_3), and 4.6 g of F127 were dissolved in 30 mL of ethanol. The synthesis was completed identically to that outlined for ZrO_2.

For the synthesis of metal phosphates, $OP(OC_2H_5)_3$ was used as a phosphorus source. For example, in the synthesis of mesoporous $4ZrO_2-P_2O_5$, 5 mmol of $OP(OC_2H_5)_3$, 10 mmol of $Zr(OBu)_4$, 40 mmol of HOAc, 24 mmol of HCl (or HNO_3), and 2.4 g of F127 were dissolved in 30 mL of ethanol. The synthesis was completed identically to that outlined for ZrO_2.

The syntheses of PbO−, BaO−, or SrO−TiO_2 composites are different from that of the previously described system. Because of the low solubility of these metal nitrate and chlorides in ethanol, neither HCl nor HNO_3 could be used to adjust system pH. Instead, metal acetates were used as precursors, and HOAc was used as the solvent instead of ethanol. For example, in the synthesis of mesoporous $PbO-TiO_2$, 10 mmol of lead acetate, 10 mmol of $Ti(OBu)_4$, and 1.8 g of F127 were dissolved in 30 mL of HOAc. The rest of the steps to make mesoporous materials are the same as those in the synthesis of mesoporous ZrO_2.

Characterization. The sizes of the inorganic species in the sol−gel solution were measured by a Malvern ZetaSizer (Nano ZS). Two-dimensional small-angle X-ray diffraction (SAXRD) patterns recorded with a custom-built diffractometer (Cu Kα radiation) were used to determine structural quality and symmetry. They were reduced to one-dimensional patterns by radial integration. Wide-angle XRD (WAXRD) patterns were recorded on a Bruker D8 diffractometer with Cu Kα radiation with a platinum heating stage. Transmission electron microscopy (TEM) images were taken using a FEI T20 electron microscope operating at 200 keV. Scanning electron microscopy (SEM) images were taken using a Philips XL30 electron microscope. Nitrogen sorption measurements were carried out at 77 K using a Micromeritics Tristar 3000 analyzer. IR spectra were collected on a Nicolet Magna 850 IR/Raman spectrometer. IR samples were prepared via mixing with KBr and pressed into pellets.

Results and Discussion

In order to quantify the growth kinetics of the oxide precursors in various environments, we use time-resolved dynamic laser light scattering (DLS, for the basic theory see

(19) Doeuff, S.; Henry, M.; Sanchez, C.; Livage, J. J. *Non-Cryst. Solids* **1987**, *89*, 206−216.
(20) Schubert, U. J. *Mater. Chem.* **2005**, *15*, 3701−3715.
(21) Brinker, C. J.; Lu, Y. F.; Sellinger, A.; Fan, H. Y. *Adv. Mater.* **1999**, *11*, 579 ff.
(22) Grosso, D.; Cagnol, F.; Soler-Illia, G.; Crepaldi, E. L.; Amenitsch, H.; Brunet-Bruneau, A.; Bourgeois, A.; Sanchez, C. *Adv. Funct. Mater.* **2004**, *14*, 309−322.

Table 1. Sizes and Growth Rates of Metal Species

	size of the inorganic species[b] (nm)		growth rate[c] (nm/min)	
inorganic species[a]	EtOH	AcHE	EtOH	AcHE
Al	$>10^3$	<1.6	1.5×10^2	4.7×10^{-4}
Si	~1.5	~1.7	1.0×10^{-3}	1.0×10^{-3}
Ti	$>10^3$	3.5	-	1.3×10^{-3}
Zr	$>10^3$	2.4	-	2.8×10^{-4}
Nb	$>10^3$	5.0	$>4.6 \times 10^2$	4.1×10^{-3}
Ta	$\sim 10^3$	8.0	41	1.2×10^{-2}
Li + Ti		7.1		1.1×10^{-2}
Ho + Ti		5.1		2.7×10^{-3}
2Al+Si		1.6		8.4×10^{-4}
Ti + P		4.6		2.7×10^{-3}
Si + Zr		3.7		3.2×10^{-3}
Ni + 2Si + 2Zr		2.6		6.7×10^{-4}
Ta + Zr		5.0		9.7×10^{-3}

[a] Al, aluminum butoxide; Si, tetraethyl silicates; Ti, titanium butoxide; Zr, zirconium butoxide; Nb, niobium ethoxide; Ta, tantalum ethoxide; Li, lithium chloride; Ni, nickel(II) nitrate; Ho, holmium chloride. [b] Size recorded at 200 min. [c] The growth rates of the metal species were determined from linear fits to the particle size plots (prior to precipitation in pure EtOH).

Supporting Information). Silicon alkoxides, for instance, are quite stable in ethanol exposed to atmospheric moisture with the particle diameter growing at a rate of 1.0×10^{-3} nm/min. However, many metal alkoxides (i.e., M= Al, Nb, or Ta) are highly reactive toward water due to coordination expansion and rapid condensation. Exposure of ethanolic solutions of these alkoxides to ambient conditions causes rapid particle growth—5 orders of magnitude faster than that of the silicon alkoxide system. Ethanolic solutions of titanium and zirconium alkoxides show an additional class of condensation kinetics—these MO particles are stable in the nanosize region for 1−2 h under ambient conditions (Figure 1a) but then rapidly grow into macro-scale precipitates.

In stark contrast to the diverse condensation and particle growth behavior observed for the metal alkoxides in ethanolic solutions, all metal alkoxides in the AcHE solution show similar condensation and particle growth behavior. In each case, nanosized metal−oxo-acetate particles form rapidly in the AcHE solution. These nanoparticles are quite stable and grow slowly due to the slow introduction of water from the ambient environment and the esterification of acetic acid.[20] Importantly, all metal species form metal oxo-acetate particles with similar sizes and growth rates (Figure 1b,c, Table 1).

DLS experiments on mixtures of MO precursors show single, well-defined nanoscale particle sizes in the AcHE solution (Figure 2). For example, isolated Ta and Zr species in the AcHE solution exhibit distinct particle sizes of 8.0 and 2.4 nm, respectively, but the AcHE solution containing the same total concentration of a mixture of Ta and Zr gives a single intermediate size (5.0 nm after 200 min) and growth rate (9.7×10^{-3} nm/min). Such behavior is consistent with the formation of a new mixed-composition nanoparticle precursor in which the Zr and Ta are interconnected via oxo/acetate bridges. We have observed similar behavior for all the mixed metal precursor systems studied (Figure 1 and Table 1), suggesting that the AcHE solution is a general route for stabilizing multicomponent oxide nanoparticle precursors, and it will be useful for the fabrication of multicomponent nanostructured materials.

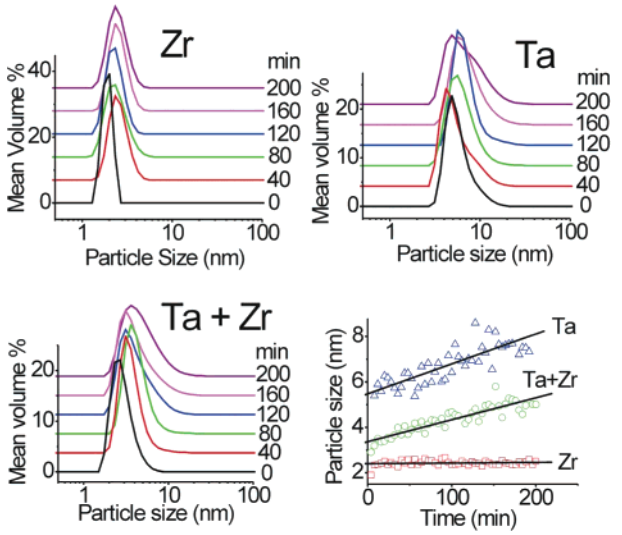

Figure 2. Size distribution and evolution of individual metal alkoxides (Ta and Zr) and their mixture in AcHE solution at room condition (25 °C, RH ~ 50%) as a function of time. In the mixture solution, M/HOAc/HCl = 1:4.0:2.1, where M = Ta + Zr (Ta/Zr = 1.0). The concentration of total metal alkoxides is 0.5 M.

Ordered mesoporous MOs (e.g., Al, Ti, Zr, Nb, and Ta) or mixed MOs (e.g., AlSi, ZrP) have been prepared via the AcHE sol−gel system using alkoxides as inorganic precursors (Table 2). For example, SAXRD patterns of mesostructured TiO_2 synthesized from titanium butoxide as the inorganic precursor and the triblock copolymer $EO_{96}PO_{70}EO_{96}$ (F127) as the template show well-resolved diffraction peaks (Figure 3a), which, when combined with TEM (Figure 4), can be unambiguously indexed as the (10) and (20) reflections of a two-dimensional hexagonal phase. The absence of the (11) reflection in the transmission-mode SAXRD pattern suggests that the one-dimensional channels are parallel to the membrane surface. The unit cell parameter calculated from SAXRD analysis are 17.4 and 12.1 nm for as-synthesized and calcined samples, respectively. Calcination of the samples at 350 °C gives rise to a relatively large cell shrinkage (as much as 30%) and broadening of the diffraction peak.

The high degree of order achievable in these multicomponent systems is apparent from the post-calcination TEM images (Figure 4). Additionally, three-dimensional cubic structures can be synthesized by tuning the volume ratio between inorganic species and the organic template. Generally, reducing the fraction of the polymer with respect to the inorganic precursors leads to cubic caged mesostructures.[23] The SAXRD patterns for the $4ZrO_2-P_2O_5$ sample synthesized from zirconium butoxide and triethyl phosphate exhibits four resolved peaks with d spacing ratios of $\sqrt{2}$:$\sqrt{4}$:$\sqrt{6}$:$\sqrt{14}$ (Figure 3b) which are indexed as the (110), (200), (211), and (321) reflections of the cubic ($Im\bar{3}m$) space group. The cell constant of the calcined sample is 12 ± 1 nm, consistent with the 11 ± 1 nm measured from TEM. Nitrogen sorption data confirm that all MOs have characteristics that are typical for mesoporous materials: uniform size distribution, high surface area, and high porosity (Table 2).

(23) Crepaldi, E. L.; Soler-Illia, G.; Grosso, D.; Cagnol, F.; Ribot, F.; Sanchez, C. *J. Am. Chem. Soc.* **2003**, *125*, 9770−9786.

Table 2. Physicochemical Properties of Mesoporous Samples

sample	organic template	calcination temperature,[a] °C	mesostructure symmetry	d_{100},[b] nm	pore size, nm	surface area, $m^2\ g^{-1}$	porosity
Al_2O_3	F127	500	*p6m*	8.1	4.4	152	0.42
TiO_2	F127	350	*p6m*	10.5	5.0	191	0.48
ZrO_2	F127	350	*p6m*	8.7	4.0	78	0.36
Nb_2O_5	F127	500	*p6m*	10.4	4.0	78	0.36
Ta_2O_5	F127	350	*p6m*	9.8	4.5	98	0.45
$4ZrO_2-P_2O_5$	F127	500	*Im*$\bar{3}$*m*	8.5	3.9	86	0.36
$2TiO_2-P_2O_5$	F127	350	disordered	11.0	3.1	305	0.48
$SiO_2-Al_2O_3$	F127	350	*p6m*	10.7	7.5	265	0.51
$MgO-TiO_2$	F127	350	*p6m*	10.6	4.0	118	0.36
$CaO-TiO_2$	F127	350	*p6m*	8.6	4.5	81	0.38
$NiO-TiO_2$	F127	350	*p6m*	10.4	4.0	186	0.46
$YbO-2TiO_2$	F127	350	*p6m*	12.3	12.0	179	0.66
$CuO-TiO_2$	Brij76	350	disordered	4.5	3.0	265	0.36
$PbO-TiO_2$	F127	350	disordered	13.0	6.5	87	0.49
$BaO-TiO_2$	P123	350	disordered	11.0	7.1	73	0.50
$NiO-2SiO_2-2ZrO_2$	F127	350	*p6m*	10.0	4.2	157	0.40
$NiO-2SiO_2-2ZrO_2$	F127	1000	*p6m*	9.7	4.2	102	0.36

[a] The wall structures of the samples are amorphous at the specified calcination temperature except for mesoporous TiO_2, whose walls consist of 7.5 nm anatase crystals, and mesoporous $NiO-2SiO_2-2ZrO_2$ calcined at 1000 °C, which contains ~5 nm tetragonal ZrO_2 nanocrystals in the walls. [b] The *d* value of the (100) reflection for samples before calcination (*d* value of the first reflection for samples with a disordered mesostructure and the *d* value of (110) for cubic phases).

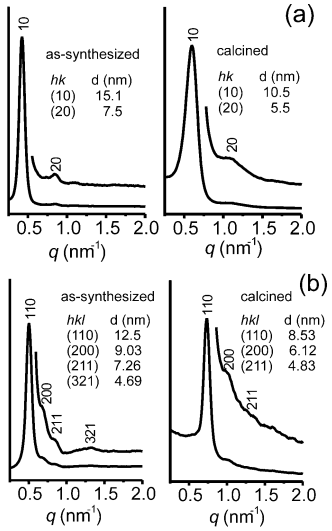

Figure 3. SAXRD patterns of mesostructured (a) TiO_2 membrane with two-dimensional hexagonal symmetry (*p6m*) and (b) $4ZrO_2-P_2O_5$ with three-dimensional cubic symmetry (*Im*$\bar{3}$*m*). The wave vector, *q*, is defined as $(4\pi/\lambda)\sin(\theta)$, where 2θ is the scattering angle. The diffracted intensity is collected in transmission geometry with respect to the planar surface of the membrane.

A variety of highly ordered mesoporous mixed MOs can be prepared by introduction of multiple transition metal and rare earth cations (e.g., Li, Mg, Ca, Cr, Co, Ni, Cu, Yb, Ho). All as-made materials show an intense low-angle diffraction peak with a *d* spacing of 14 to 18 nm, indicating mesoscopic ordering for all samples (Supporting Information). Removal of the surfactants by combustion at 350 °C generally causes cell shrinkage of ~30%. TEM reveals ordered mesopore arrays throughout the specimen domain of the calcined sample. WAXRD confirms that most oxide frameworks are amorphous at the atomic scale when calcined at an intermediate temperature (350 °C; Table 2).

The incorporation of Pb, Sr, and Ba ions is more difficult than that for other transition metal cations because of the low solubility of the chloride and nitrate salts in ethanol solution. Additionally, neither HCl nor HNO_3 is suitable as a strong acid due to the low solubility of the metal nitrates or chlorides of these ions. This problem is resolved in our approach by using glacial acetic acid as the solvent and elevating the solution temperature. A strong but relatively broad X-ray diffraction peak is observed for $PbO-TiO_2$, $BaO-TiO_2$, and $SrO-TiO_2$ samples (Supporting Information). TEM analysis indicates a disordered worm-like structure. The absence of mesoscopic ordering confirms that a stronger charge interaction between inorganic and organic species is required for cooperative assembly.

A homogeneous distribution of each component is an important issue for MMMOs, as the dispersion of individual elements can greatly influence performance in catalytic, optical, and electronic applications. The uniform unimodal size distribution in the nanorange (1−10 nm) of mixed metal species in the AcHE sol−gel system suggests that a high homogeneity at the nanoscale in the final product can be obtained. A detailed energy dispersive X-ray (EDX) element mapping measurement of ternary mesoporous MO ($NiO-2SiO_2-2ZrO_2$) shows uniform intensity of Ni, Si, and Zr signals throughout the particles (Supporting Information), revealing the homogeneous distribution of multiple components within the inorganic framework. The molar ratio of Ni:Si:Zr determined from EDX was 1.19:1.96:2.00—close to the actual composition of the precursor solution (1:2:2).

We have studied the wall phase segregation and crystallization behavior of the mesoporous $NiO-2SiO_2-2ZrO_2$ system in detail. Temperature-dependent WAXRD data reveal the componential segregation and crystallization behavior of this ternary composite (Figure 5). Between room temperature and 800 °C the sample remains amorphous. After heating at 900 °C, the zirconia component in the mesophase crystallizes into a tetragonal phase, as indicated by the presence of the (101) peak at $2\theta = 29.8°$; the other components, however, remain amorphous. The crystal size of tetragonal zirconia is calculated to be ~5.3 nm based on WAXRD peak broadening by the Scherer formula. A further increase in the temperature to 1000 °C does not cause additional crystal growth. SAXRD and TEM investigation confirm the preservation of mesoscopic ordering even after heating at 1000 °C. High-resolution TEM reveals crystallized

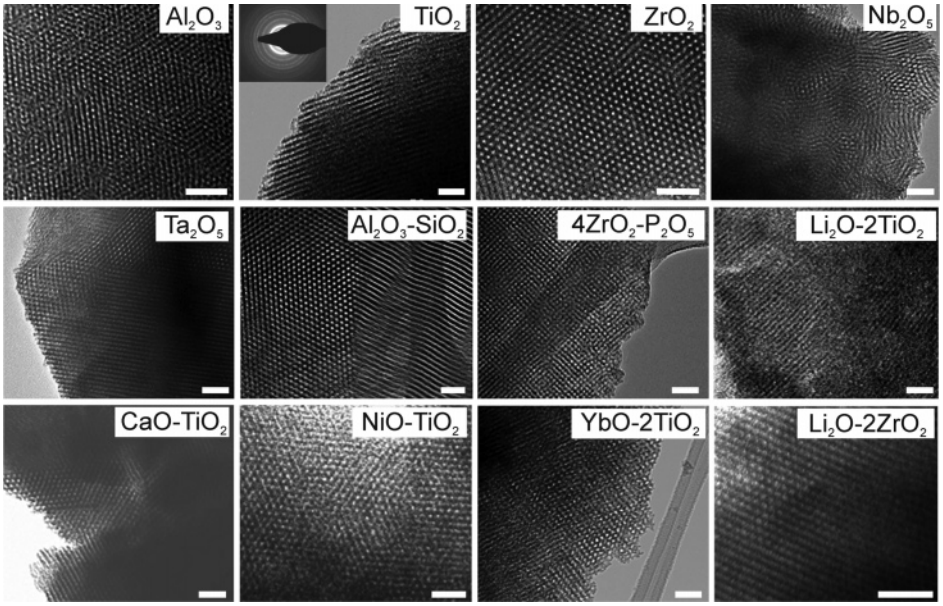

Figure 4. TEM images of calcined mesoporous materials. Mesoporous MOs are calcined at 350 °C in air for 5 h to remove organic polymer templates (Al_2O_3, Nb_2O_5, and $4ZrO_2-P_2O_5$ samples are calcined at 500 °C). Selected-area electron diffraction confirms that mesoporous TiO_2 contains crystalline (anatase) pore walls after calcination. The scale bar in each case is 50 nm.

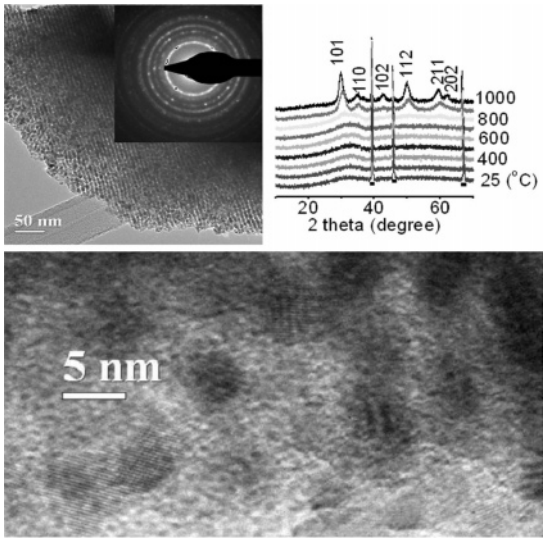

Figure 5. WAXRD patterns of a ternary mesoporous $NiO-2SiO_2-2ZrO_2$ sample at different heating temperatures and TEM images of the specimen heated at 1000 °C. The presence of ~5 nm zirconia nanocrystals in the wall structure is evident from the selected area diffraction pattern, the high-resolution TEM image, and the WAXRD patterns. The sharp peaks marked with ■ correspond to diffraction from the platinum heating stage.

zirconia nanoparticles with a size of ~5 nm that are uniformly embedded in one-dimensional channel walls (Figure 5). This material has a pore size of ~4.2 nm and a surface area 102 m^2 g^{-1} (Table 2 and Supporting Information).

Single component mesoporous zirconia shows a clear amorphous-to-tetragonal phase transition at 450 °C, with large (14 nm) zirconia nanocrystals forming alongside the collapse of the ordered mesostructure by 500 °C (Supporting Information). This behavior is in sharp contrast to the multicomponent $NiO-2SiO_2-2ZrO_2$ hybrid (Ni:Si:Zr = 1:2:2 molar ratio). These differences in wall structural stability are associated with the interfaces between different components in mesoporous $NiO-2SiO_2-2ZrO_2$; these interfaces suppress the crystallization and growth of individual components by limiting mass diffusion.[24] Both NiO and ZrO_2 are particularly interesting for catalytic use in chemical and petrochemical processes because of their acidic, basic, and redox properties.[25,26] This mesoporous multicomponent $NiO-2SiO_2-2ZrO_2$ is expected to be a promising catalytic system because of the homogeneous dispersion of each component, existence of tetragonal ZrO_2 nanocrystals, and silica-stabilized mesoporous frameworks.

In the AcHE sol−gel system, acetic acid plays a key role in adjusting the growth of inorganic species and formation of stable nanoparticles. For instance, carboxylic acids have previously been used as complexing ligands to modify titania sol−gel processing.[19] Thermogravimetric analysis reveals that a substantial number of acetate groups are retained in each single or multicomponent mesostructured hybrid before aging at 65 °C (0.40 to 1.86 acetate groups per metal atom; Supporting Information). IR spectroscopy suggests that these acetate groups act as bidentate ligands, which are directly bonded to the metal ions through chelating or bridging modes (Supporting Information). As a result of carboxylate binding the reactivity toward water of modified metal species is greatly decreased, which leads to controlled precursor particles sizes and condensation kinetics.[19,20] Most importantly, the diverse condensation kinetics of a variety of metal species are normalizalized within a narrow range and, thus, make possible the synthesis of mesostructured materials with complicated MO stoichiometries. These facts also distinguish the approach from previous metal chloride precursor routes for the synthesis of mesoporous MOs.[7,27] In the metal chloride precursor solution, inorganic species remain as monomers or small oligomers, less than 0.6 nm as indicated

(24) Li, D. L.; Zhou, H. S.; Honma, I. *Nat. Mater.* **2004**, *3*, 65−72.
(25) Mango, F. D. *Org. Geochem.* **1996**, *24*, 977−984.
(26) Postula, W. S.; Feng, Z. T.; Philip, C. V.; Akgerman, A.; Anthony, R. G. *J. Catal.* **1994**, *145*, 126−131.
(27) Grosso, D.; Soler-Illia, G.; Babonneau, F.; Sanchez, C.; Albouy, P. A.; Brunet-Bruneau, A.; Balkenende, A. R. *Adv. Mater.* **2001**, *13*, 1085 ff.

by our DLS experiments, during the assembly process. This explains why the metal−chloride-based method often requires long gelation times (up to 2 weeks) to obtain stable mesostructures in macroscopic samples. For thin films on the order of several hundred nanometers thick, the evaporation of HCl drives the condensation reactions more rapidly.[23,28] Our method is also distinct from previously reported nanoparticle based routes to mesostructured materials, where separately synthesized precrystallized nanoparticles are assembled into high-surface-area and thermally stable mesostructures; in our case, the nanoparticle precursors are generated in situ by controlling the sol−gel process.[29,30] This has the advantage of making the synthesis extremely simple and general, but the possible disadvantage is that the initially formed materials are amorphous at the atomic level. However, for catalytic applications, the ability to introduce multiple catalytic MO components into accessible wall structures may be much more important than framework crystallization.

The modification of metal alkoxides by acetic acid influences the structural properties of the final material. The degree of cross-linking of the metal gel networks is decreased because of the replacement of hydrolyzable alkoxy groups by acetate groups. Additionally, the density of the gel networks is lower than that of the pure oxide frameworks due to the substantial proportion of bridging or chelating acetate groups. These less-condensed gel networks cannot sustain their mesoscopic order after removal of organic templates by calcination. An additional aging step is therefore required to condense the frameworks. For example, it was found that the number of acetate groups per titanium decreased from 1.10 to 0.57 after aging at 65 °C for 24 h (for aluminum, it decreases from 0.40 to 0.16). After aging, the materials can retain their original mesostructures after surfactant removal. Previously, we have used trifluoroacetic acid to synthesize nonporous titania-based hybrid optical materials.[16] Compared to the trifluoroacetate-modified titania system, in which small oligomers (∼four to five Ti atoms) are formed in solution, weaker-binding non-fluorinated acetate ligands allow the growth of larger nanometer-sized inorganic particles. Because acetate ligands are both smaller and weaker binding, they are also readily removed during heat treatment to yield desirable *mesoporous* oxides.

Conclusions

In summary, we have described a simple and widely applicable methodology for the synthesis of multicomponent mesostructured hybrids and porous materials from the combination of inexpensive and commercially available polymers with metal alkoxides solubilized in the AcHE solution. MMMOs obtained by the AcHE system have tunable pore structures, multiple components, a high degree of homogeneity, and, in certain cases, thermal stability above 1000 °C. The ability to easily process these diverse MMMOs in the form of thin films, free-standing membranes, and monoliths (Supporting Information) presents substantial advantages over previously reported methods for commercial applications in heterogeneous catalysts, energy storage, photocatalysis, or nanostructured photovoltaics, where large quantities of material will be required.[7,27] Most importantly, we have demonstrated that, using this method, the diverse condensation kinetics of a variety of MO materials can be homogenized to yield stable multicomponent MO nanoparticle precursors. The development of such simple and widely applicable methodologies for the fabrication of novel MMMOs (e.g., rare earth and transition MOs) with diverse compositions is important for the practical implementation of these nanostructured materials.

Acknowledgment. We thank Dr. Nanfeng Zheng, Dr. Yiying Wu, Dr. Jianfang Wang, Martin Schierhorn, and Chiakuang (Frank) Tsung for their contributions. This work was supported in part by the National Science Foundation under Grant DMR 02-33728 and made use of MRL Central Facilities supported by the MRSEC program of the National Science Foundation under Award No. DMR05-20415. S.W.B. acknowledges the NSF for a Graduate Research Fellowship.

Supporting Information Available: Additional characterization data (DSL, SEM, IR, SAXS, and XRD; PDF). This material is available free of charge via the Internet at http://pubs.acs.org.

CM062359D

(28) Yang, P.; Zhao, D.; Margolese, D. I.; Chmelka, B. F.; Stucky, G. D. *Chem. Mater.* **1999**, *11*, 2813−2826.
(29) Corma, A.; Atienzar, P.; Garcia, H.; Chane-Ching, J. Y. *Nat. Mater.* **2004**, *3*, 394−397.
(30) Wong, M. S.; Jeng, E. S.; Ying, J. Y. *Nano Lett.* **2001**, *1*, 637−642.